arXiv:1408.1408v2 [cond-mat.str-el] 10 Oct 2014

Orbital Nematic Order and Interplay with Magnetism in the Two-Orbital Hubbard Model

Zhentao Wang[1] and Andriy H. Nevidomskyy[1]

[1]*Department of Physics and Astronomy, Rice University, Houston, TX 77005*

Motivated by the recent angle-resolved photoemission spectroscopy (ARPES) on FeSe and iron pnictide families of iron-based superconductors, we have studied the orbital nematic order and its interplay with antiferromagnetism within the two-orbital Hubbard model. We used random phase approximation (RPA) to calculate the dependence of the orbital and magnetic susceptibilities on the strength of interactions and electron density (doping). To account for strong electron correlations not captured by RPA, we further employed non-perturbative variational cluster approximation (VCA) capable of capturing symmetry broken magnetic and orbitally ordered phases. Both approaches show that the electron and hole doping affect the two orders differently. While hole doping tends to suppress both magnetism and orbital ordering, the electron doping suppresses magnetism faster. Crucially, we find a realistic parameter regime for moderate electron doping that stabilizes orbital nematicity in the absence of long-range antiferromagnetic order. This is reminiscent of the non-magnetic orbital nematic phase observed recently in FeSe and a number of iron pnictide materials and raises the possibility that at least in some cases, the observed electronic nematicity may be primarily due to orbital rather than magnetic fluctuations.

I. INTRODUCTION

Nematicity, defined as spontaneous breaking of the four-fold rotational C_4 symmetry down to C_2, has been recently observed in the electronic properties of Fe-based superconductors[1,2]. Experimental efforts, including transport measurements[3–10], optical conductivity[4,11–13], scanning tunneling microscopy[14–16], neutron scattering[17–19], quantum oscillations[20], magnetic torque measurements[21], and angle-resolved photoemission spectroscopy (ARPES) measurements[22–24], have reported the electronic in-plane anisotropy, mostly in the compounds of the $BaFe_2As_2$ (122) family, even at temperatures higher than the lattice structural transition[3,8,19,21,23,24]. Upon electron doping, the resistivity anisotropy is first enhanced in the underdoped region, but then suppressed upon further doping into the superconducting region[3]; while hole doping appears to suppress the resistivity anisotropy even while below the structural phase transition[7].

Origins of the observed anisotropy have been discussed in the context of lattice, magnetic and orbital fluctuations[25–35], and there are also debates whether the nematicity is intrinsic or if it comes from the anisotropic impurity scattering[10,16,36]. Recent resistivity ρ measurements under fixed strain[8] $\delta = (a-b)/(a+b)$ (a and b are the lattice constants) have detected divergent nematic susceptibility $\mathrm{d}\rho/\mathrm{d}\delta$, proving that the nematicity is of electronic origin rather than due to an elastic lattice instability.

One possible mechanism behind this electronic nematicity is the so-called Ising-nematic (also referred to as "spin nematic") scenario, based on the discrete Ising symmetry breaking between two columnar antiferromagnetic (CAF) ordering wave-vectors, $\mathbf{Q}_1 = (\pi, 0)$ and $\mathbf{Q}_2 = (0, \pi)$. In the ordered CAF phase, the magnetization $\mathbf{M}(r) = \mathbf{M}_1 e^{i\mathbf{Q}_1\cdot\mathbf{r}} + \mathbf{M}_2 e^{i\mathbf{Q}_2\cdot\mathbf{r}}$ breaks the C_4 symmetry whenever $M_1 \neq M_2$, and neutron scattering finds either $M_1 = 0$ or $M_2 = 0$ in the iron pnictides[17,37]. The nematic order parameter is defined as the difference in spin correlations along the $\hat{x}$ and $\hat{y}$ axes:

$$\psi = \sum_i |\mathbf{M}(i)\cdot\mathbf{M}(i+\hat{x}) - \mathbf{M}(i)\cdot\mathbf{M}(i+\hat{y})| \propto |M_1|^2 - |M_2|^2. \quad (1)$$

However, the C_4 symmetry can be spontaneously broken even above the Néel temperature (T_N) due to anisotropic spin fluctuations, as was first pointed out by Chandra, Coleman and Larkin[38], and later applied to the iron pnictides[25–27,39,40]. Recently, these anisotropic spin fluctuations have been imaged directly[19] using the inelastic neutron scattering in uniaxial-pressure detwinned samples of $BaFe_{2-x}Ni_xAs_2$.

On the other hand, it has been proposed that the electronic nematicity may stem from unequal population of the d_{xz} and d_{yz} orbitals, resulting in the ferro-orbital ordering[28–33]. The order parameter is the orbital polarization $p = \langle n_{xz} - n_{yz}\rangle$, which explicitly breaks the C_4 symmetry. Experimentally, polarization-dependent ARPES found orbitally-polarized Fermi surfaces inside the CAF phase of the parent compound $BaFe_2As_2$[22]. The unambiguous splitting of Fe d_{xz} and d_{yz} orbitals has also been observed by ARPES above the structural transition temperature T_s in the detwinned samples of lightly Co-doped[23] and P-doped[24] $BaFe_2As_2$.

The driving force for the electronic nematic transition is very difficult to determine because of the strong coupling between internal spin and orbital degrees of freedom. Indeed, on the symmetry grounds, Landau free energy will contain a linear coupling between the Ising-nematic order parameter ψ and the orbital ordering p:

$$\Delta F = \eta\, p\cdot\psi \;\propto\; \eta\, p\cdot\left\langle M_1^2 - M_2^2\right\rangle. \quad (2)$$

Independent of the sign of the coupling constant η, such a term in the free energy will result in a non-vanishing value of the orbital polarization whenever ψ takes on a non-zero value, and the other way round. It has been proposed that this "chicken and egg" problem may in principle be resolved by comparing the rates of divergence in the orbital and Ising-spin susceptibilities on approaching the transition,[41] however this approach would only work provided the coupling constant $|\eta|$ is not too large. In this study, we aim to address a different question, namely, is it possible, and under what conditions, to stabilize a static ferro-orbital order in the absence of long-range magnetic ordering?

In order to disentangle the effects of the magnetic and orbital ordering, it is useful to consider the compounds where the two phases are clearly separated. One such example is

NaFeAs of the 111 family with $T_s = 53$ K significantly higher than the Néel temperature $T_N = 40$ K. Recent ARPES measurements in NaFeAs indicate[42,43] that the orbital order develops exactly at or slightly above T_s and appears to trigger the antiferromagnetic order at the lower temperature T_N, due to the nesting of the two-fold anisotropic Fermi surface[42]. One is tempted therefore to interpret this result based on the orbital-driven scenario[42]. Intriguingly, scanning tunneling spectroscopy finds evidence of local electronic nematicity up to temperatures twice T_s, in the nominally tetragonal phase[44].

An even clearer signature of the orbital ordering in the absence of magnetism is observed in stoichiometric FeSe, which undergoes a structural transition at around $T_s \approx 90$ K without any sign of the antiferromagnetic ordering[45,46]. Recent ARPES measurements[47] on FeSe show a clear splitting of ~ 50 meV between the energies of the Fe d_{xz} and d_{yz} orbital bands, which sets in at about T_s. Importantly, this measured energy splitting is more than five times larger than expected from density-functional theory (DFT) calculations considering the orthorhombic lattice distortion alone[47]. The likely orbital nature of the structural transition in FeSe is also corroborated by recent nuclear magnetic resonance (NMR)[48,49] and shear modulus measurements[49].

The above experimental observations raise a possibility that it may indeed be possible to stabilize ferro-orbital order in the absence of long-range magnetic ordering. It is the purpose of this article to address this question theoretically within the minimal two-orbital model.[50,51] While the two-orbital model is known to have a number of limitations in describing the iron-based superconductors (for instance, resulting in a wrong number of Fermi pockets and missing the d_{xy} orbital contents on the Fermi surface), the primary reason for using this model here is its conceptual simplicity. We do not presume that such a simple model can describe the realistic electronic properties of, e.g. FeSe or LiFeAs. Rather, the question we aim to address can be phrased as follows – what is the minimal theoretical model (whether or not applicable to the iron pnictides) that can support orbital nematic ordering in the absence of magnetism? In this article, we show that the two-orbital model is sufficient to describe this physics under realistic values of intra-orbital and inter-orbital Coulomb repulsion. Generalization of these results to a realistic five-orbital model of the iron pnictides or iron chalcogenided will be the subject of future work.

We used the combination of RPA and non-perturbative quantum cluster calculations (VCA) to study the effect of electron interactions and doping on both the antiferromagnetism and ferro-orbital ordering. Within the two-orbital model, we find that the orbital nematic order strongly depends on inter-orbital Hubbard repulsion and Hund's coupling term, and its dependence on electron and hole doping is not symmetric. In the undoped and hole-doped system, we find that orbital order coexists with magnetic order, as observed ubiquitously in the 122 family of iron pnictides. Our key finding is that sufficient electron doping stabilizes the orbital nematic phase while suppressing the antiferromagnetic ordering, suggestive of the experimental observations of orbital order in Co-doped LiFeAs[52] and FeSe[47**?** ,48].

This paper is organized as follows: In Section II we introduce the two-orbital Hubbard model as a starting point for our calculations; in Section III and IV we study the orbital nematic order and its interplay with the magnetic order by using RPA and VCA methods, respectively; in Section V, we discuss our results in the context of the related theoretical and experimental work, and we finally draw the conclusions in Section VI.

II. MODEL

To study the orbital nematic order in Fe-based superconductors, we start from the minimal two-orbital Hubbard model capturing the itinerant electrons with onsite electron-electron interactions:

$$\begin{aligned} H = H_0 &+ U \sum_{i,\alpha} n_{i\alpha\uparrow} n_{i\alpha\downarrow} + (U' - \frac{J}{2}) \sum_{i,\alpha<\beta} n_{i\alpha} n_{i\beta} \\ &- 2J \sum_{i,\alpha<\beta} \boldsymbol{S}_{i\alpha} \cdot \boldsymbol{S}_{i\beta} + J' \sum_{i,\alpha<\beta} (c^\dagger_{i\alpha\uparrow} c^\dagger_{i\alpha\downarrow} c_{i\beta\downarrow} c_{i\beta\uparrow} + h.c.) \end{aligned} \tag{3}$$

Here i is the site label, $\alpha, \beta \in \{xz, yz\}$ stand for the orbital indices. U and U' are respectively the intra- and inter-orbital Hubbard interaction, J stands for the Hund's coupling and $J' = J$ stands for the pair hopping term. H_0 is the non-interacting two-orbital Hamiltonian from Ref. 50:

$$H_0 = \sum_{\boldsymbol{k}\sigma} \psi^\dagger_{\boldsymbol{k}\sigma} [\epsilon_+(\boldsymbol{k}) \mathbb{1} + \epsilon_-(\boldsymbol{k}) \tau_3 + \epsilon_{xy}(\boldsymbol{k}) \tau_1] \psi_{\boldsymbol{k}\sigma} \tag{4}$$

with $\psi^\dagger_{\boldsymbol{k}\sigma} = [c^\dagger_{xz,\sigma}(\boldsymbol{k}), c^\dagger_{yz,\sigma}(\boldsymbol{k})]$, where σ is the spin label, and

$$\begin{aligned} \epsilon_\pm(\boldsymbol{k}) &= \frac{\epsilon_x(\boldsymbol{k}) \pm \epsilon_y(\boldsymbol{k})}{2} \\ \epsilon_x(\boldsymbol{k}) &= -2t_1 \cos k_x - 2t_2 \cos k_y - 4t_3 \cos k_x \cos k_y \\ \epsilon_y(\boldsymbol{k}) &= -2t_2 \cos k_x - 2t_1 \cos k_y - 4t_3 \cos k_x \cos k_y \\ \epsilon_{xy}(\boldsymbol{k}) &= -4t_4 \sin k_x \sin k_y \end{aligned} \tag{5}$$

The values of the hopping parameters have been kept fixed throughout the context: $t_1 = -0.25eV, t_2 = 0.325eV, t_3 = t_4 = -0.2125eV$.

The reason behind studying the two-orbital (as opposed to the full five-orbital) model is the universally accepted fact that the major contribution to the Fermi surface comes from the iron t_{2g} orbitals (d_{xz}, d_{yz}, d_{xy}), whereas the e_g orbital weight is very small[53,54]. Additionally, the d_{xz} and d_{yz} orbitals carry most of the spectral weight[53] and the d_{xy} orbital can thus be neglected in the first approximation. While it is true that in order to obtain *all* the Fermi pockets observed in ARPES, one needs to consider all 5 Fe orbitals[55], here we chose to focus on the two-orbital model in the hope that it captures the salient features of nematicity in the iron pnictides, especially because the ferro-orbital nematic order only affects the two d_{xz} and d_{yz} orbitals in question. We expect that our central results will remain unaltered upon inclusion of the other orbitals, however demonstrating this explicitly will be the subject of future work. We note that the present approach is similar in spirit to the weak-coupling approaches[40,56–58] which start from the

band picture of a hole pocket around the Γ-point and electron pockets in the corners of the Brillouin zone, in a sense that these approaches also deal with a reduced Hilbert space of typically two bands (irrespective of their orbital contents). Nevertheless, even such a simplified two-band approach is known to produce reliable results which are largely unaffected by inclusion of other bands[58].

We point out that another, more pragmatic reason for limiting the present consideration to two orbitals is because the five-orbital model is well beyond the computational demands of the state-of-the-art variational cluster approximation used in this work (see section IV for more detail). Studying antiferromagnetism necessitates the use of a 4-site cluster, which when combined with 5 orbitals per Fe site, would result in an effective 20-"site" Hubbard model that lies well beyond the present limits of either the exact diagonalization or continuous-time quantum Monte Carlo solver[59] used in VCA or in cluster-DMFT.

The inter- and intra-orbital interaction strengths in Eq. (3) are not independent of each other. In the atomic limit, a well known relation $U' = U - 2J$ holds, which ensures orbital rotational invariance[60]. In a solid, the electron-electron interactions are screened, meaning that the above relation between U' and U may not be obeyed exactly. Below, we shall investigate the phase diagram of the model Eq. (3) treating U' and U as independent parameters. However later on, when studying the effect of interactions on nematicity and antiferromagnetism, we shall use the relation $U' = U - 2J$ which we expect to hold approximately in the iron pnictides. The values of interactions for the 122 Fe-pnictides in the two-orbital model are approximately $U = 2$ eV, $U' = 0.6$ eV, $J = 0.7$ eV. Note that we chose the interaction U to be somewhat lower than $U = 2.7$ eV calculated within the *ab initio* constrained-RPA scheme[61], which is consistent with the smaller effective bandwidth when considering only d_{xz} and d_{yz} orbitals in Eq. (3), compared to the width of all 5 Fe bands. When we attempted to use larger values of $U \gtrsim 2.5$ eV, the variational cluster calculations (see Sec. IV below) indicate the parent compound to be a Mott insulator. Therefore, to keep the system metallic in agreement with experiments, we were forced to choose a lower value of $U = 2$ eV.

III. RANDOM PHASE APPROXIMATION

For the case when interaction is not too strong, we can treat the Hubbard terms and Hund's term as perturbation, and do an RPA calculation for both the spin-spin correlation function and orbital nematic density-density correlation function:

$$\chi_{spin}(\boldsymbol{k}, i\omega_n) \equiv 2\int_0^\beta d\tau \sum_{\alpha_1\alpha_2}\sum_{\boldsymbol{r}} e^{i\omega_n\tau - i\boldsymbol{k}\cdot\boldsymbol{r}}\langle T\hat{\boldsymbol{S}}^z_{\alpha_1}(\boldsymbol{r},\tau)\hat{\boldsymbol{S}}^z_{\alpha_2}(\boldsymbol{0},0)\rangle \quad (6)$$

$$\chi_{nematic}(\boldsymbol{k}, i\omega_n) \equiv \frac{1}{2}\int_0^\beta d\tau \sum_{\boldsymbol{r}} e^{i\omega_n\tau - i\boldsymbol{k}\cdot\boldsymbol{r}}\langle T(\hat{n}_{xz}(\boldsymbol{r},\tau) - \hat{n}_{yz}(\boldsymbol{r},\tau))\cdot (\hat{n}_{xz}(\boldsymbol{0},0) - \hat{n}_{yz}(\boldsymbol{0},0))\rangle \quad (7)$$

Where α_1, α_2 are orbital indices. Summation over spin indices has been made implicit by writing $\hat{n}_\alpha = \hat{n}_{\alpha\uparrow} + \hat{n}_{\alpha\downarrow}$.

The bare spin and orbital nematic susceptibilities are of the form:

$$\chi^{(0)}_{spin}(\boldsymbol{k}, i\omega_n) = \frac{-1}{2\beta\mathcal{N}}\sum_{\omega_m,\boldsymbol{q}} \mathrm{Tr}[\sigma^z_{s_1s_2}\tilde{G}^{\alpha_1\alpha_2}_0(\boldsymbol{k}+\boldsymbol{q}, i\omega_n + i\omega_m)\sigma^z_{s_1s_2}\tilde{G}^{\alpha_2\alpha_1}_0(\boldsymbol{q}, i\omega_m)] = -\left(D^{xx}_0(\boldsymbol{k}, i\omega_n) + D^{yy}_0(\boldsymbol{k}, i\omega_n) + 2D^{xy}_0(\boldsymbol{k}, i\omega_n)\right) \quad (8)$$

$$\chi^{(0)}_{nematic}(\boldsymbol{k}, i\omega_n) = \frac{-1}{2\beta\mathcal{N}}\sum_{\omega_m,\boldsymbol{q}} \mathrm{Tr}[\tau^z_{\alpha_1\alpha_2}\tilde{G}^{\alpha_1\alpha_4}_0(\boldsymbol{k}+\boldsymbol{q}, i\omega_n + i\omega_m)\tau^z_{\alpha_3\alpha_4}\tilde{G}^{\alpha_3\alpha_2}_0(\boldsymbol{q}, i\omega_m)] = -\left(D^{xx}_0(\boldsymbol{k}, i\omega_n) + D^{yy}_0(\boldsymbol{k}, i\omega_n) - 2D^{xy}_0(\boldsymbol{k}, i\omega_n)\right) \quad (9)$$

Where trace is over both spin and orbital indices. $\tilde{G}^{\alpha\beta}_0$ is the non-interacting Green's function. $D^{\alpha\beta}_0(\boldsymbol{k}, i\omega_n)$ is the 2×2 matrix standing for the bare bubble, and $\alpha, \beta = x, y$ stand for xz, yz orbitals:

$D^{\alpha\beta}_0(\boldsymbol{k}, i\omega_n) =$

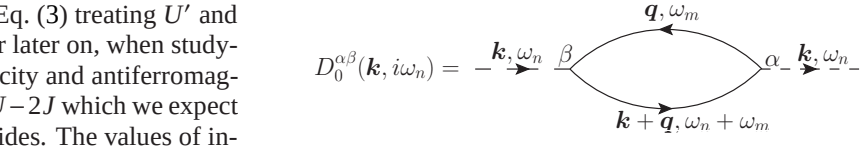

$$= \frac{1}{\mathcal{N}}\sum_{\boldsymbol{q}}\sum_{\nu_1\nu_2}\langle\alpha|\nu_1, \boldsymbol{k}+\boldsymbol{q}\rangle\langle\nu_1, \boldsymbol{k}+\boldsymbol{q}|\beta\rangle\langle\beta|\nu_2, \boldsymbol{q}\rangle\langle\nu_2, \boldsymbol{q}|\alpha\rangle \cdot \frac{n_F(E_{\boldsymbol{q},\nu_2}) - n_F(E_{\boldsymbol{k}+\boldsymbol{q},\nu_1})}{i\omega_n + E_{\boldsymbol{q},\nu_2} - E_{\boldsymbol{k}+\boldsymbol{q},\nu_1}} \quad (10)$$

where ν_1, ν_2 are band indices, and $E_{\nu,\boldsymbol{q}}$ is the dispersion of the two non-interacting bands.[50]

$$E_\pm(\boldsymbol{k}) = \epsilon_+(\boldsymbol{k}) \pm \sqrt{\epsilon^2_-(\boldsymbol{k}) + \epsilon^2_{xy}(\boldsymbol{k})} \quad (11)$$

The matrix form of the bare spin and orbital nematic susceptibilities are as follows:

$$(\chi^{(0)}_{spin}) = \begin{pmatrix} \chi^{(0)}_{xx} & \chi^{(0)}_{xy} \\ \chi^{(0)}_{yx} & \chi^{(0)}_{yy} \end{pmatrix}_{spin} = -\begin{pmatrix} D^{xx}_0 & D^{xy}_0 \\ D^{yx}_0 & D^{yy}_0 \end{pmatrix} \quad (12)$$

$$(\chi^{(0)}_{nematic}) = \begin{pmatrix} \chi^{(0)}_{xx} & \chi^{(0)}_{xy} \\ \chi^{(0)}_{yx} & \chi^{(0)}_{yy} \end{pmatrix}_{nematic} = -\begin{pmatrix} D^{xx}_0 & -D^{xy}_0 \\ -D^{yx}_0 & D^{yy}_0 \end{pmatrix} \quad (13)$$

When taking interactions into consideration, we sum over the RPA series of diagrams for the two susceptibilities, see Figs. 1 and 2.

Then RPA-renormalized spin and orbital susceptibilities take the form:

$$(\chi_{spin}) = (\chi^{(0)}_{spin})\left(\mathbb{1} - \begin{pmatrix} U & J \\ J & U \end{pmatrix}(\chi^{(0)}_{spin})\right)^{-1} \quad (14)$$

$$(\chi_{nematic}) = (\chi^{(0)}_{nematic})\left(\mathbb{1} + \begin{pmatrix} U & -2U'+J \\ -2U'+J & U \end{pmatrix}(\chi^{(0)}_{nematic})\right)^{-1} \tag{15}$$

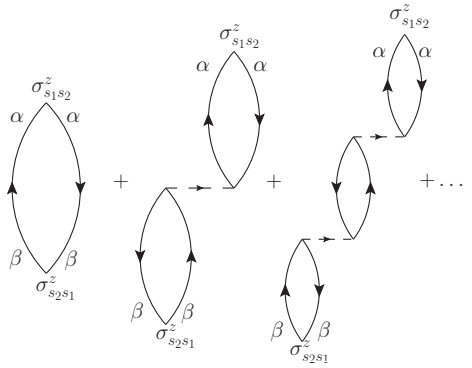

FIG. 1. RPA diagrams for spin susceptibility.

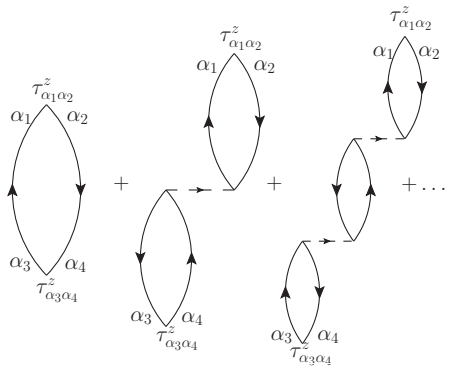

FIG. 2. RPA diagrams for orbital nematic susceptibility.

When we sum over all components of the matrices, we get the total RPA-renormalized susceptibilities in the scalar form:

$$\begin{aligned}
&\chi_{spin}(\boldsymbol{k}, i\omega_n) \\
&= \chi_{xx}(\boldsymbol{k}, i\omega_n) + \chi_{xy}(\boldsymbol{k}, i\omega_n) + \chi_{yx}(\boldsymbol{k}, i\omega_n) + \chi_{yy}(\boldsymbol{k}, i\omega_n) \\
&= \left[\chi^{(0)}_{spin}(\boldsymbol{k}, i\omega_n) - 2(U-J)\det D_0(\boldsymbol{k}, i\omega_n)\right] / \Big\{1 - U\chi^{(0)}_{spin}(\boldsymbol{k}, i\omega_n) \\
&\quad -2(U-J)D_0^{xy}(\boldsymbol{k}, i\omega_n) + (U^2 - J^2)\ \det D_0(\boldsymbol{k}, i\omega_n)\Big\}
\end{aligned} \tag{16}$$

$$\begin{aligned}
&\chi_{nematic}(\boldsymbol{k}, i\omega_n) \\
&= \left[\chi^{(0)}_{nematic}(\boldsymbol{k}, i\omega_n) + 2(U+2U'-J)\det D_0(\boldsymbol{k}, i\omega_n)\right] / \Big\{1 + \\
&\quad U\chi^{(0)}_{nematic}(\boldsymbol{k}, i\omega_n) + 2(U-2U'+J)D_0^{xy}(\boldsymbol{k}, i\omega_n) + \\
&\quad [U^2 - (2U'-J)^2]\ \det D_0(\boldsymbol{k}, i\omega_n)\Big\}
\end{aligned} \tag{17}$$

Where $\chi^{(0)}_{spin}$ and $\chi^{(0)}_{nematic}$ are defined in Eq. 8 and Eq. 9, and $\det D_0 = D_0^{xx}D_0^{yy} - D_0^{xy}D_0^{yx}$.

From the expression of $D_0^{\alpha\beta}$ (see Eq. 10), $\mathrm{Re}D_0^{\alpha\beta} < 0$ in general. We also notice that at $\boldsymbol{q} = 0$, $\det D_0(\boldsymbol{0}, \omega) > 0$, thus the ferro orbital nematic instability comes from the

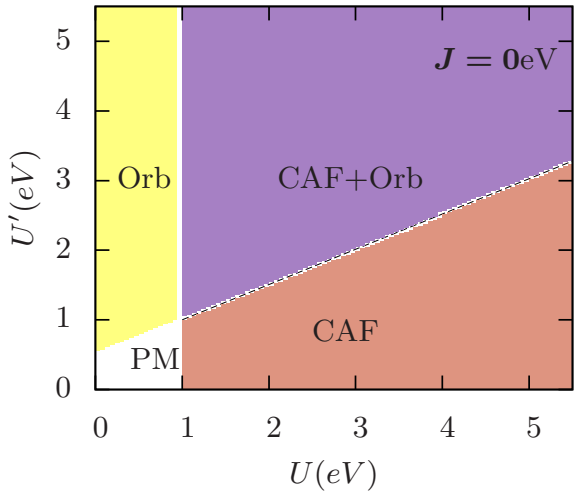

FIG. 3. (Color online) RPA phase diagram when fixing $J = 0$ and $\mu = 0.3625$eV. Phases PM, CAF and Orb respectively denote the isotropic paramagnetic phase, the columnar antiferromagnetic phase, and the orbital nematic phase.

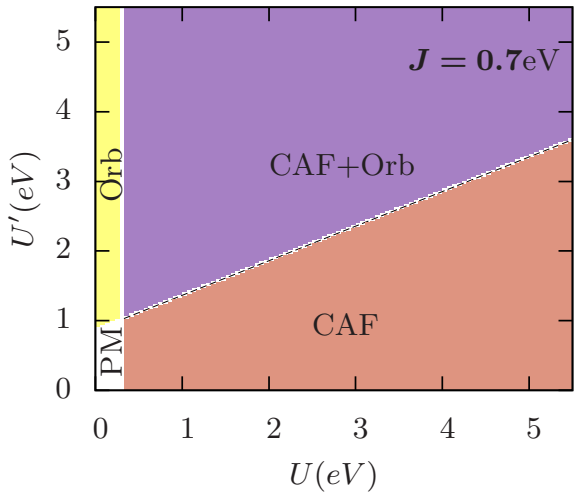

FIG. 4. (Color online) RPA phase diagram when fixing $J = 0.7eV$ and $\mu = 0.3625$eV. Phases PM, CAF and Orb using same abbreviation as in Fig. 3

$-(2U'-J)^2\ \det D_0$ term, ie. the orbital nematic susceptibility at $\boldsymbol{q} = 0$ only diverges when we have large enough inter-orbital Hubbard repulsion, and Hund's coupling cannot be too large.

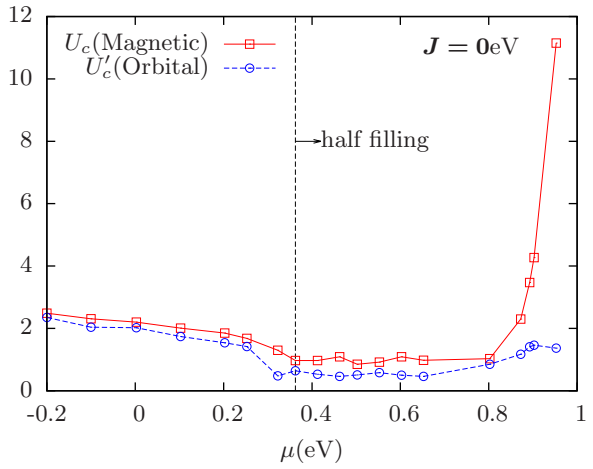

FIG. 5. (Color online) The dependence of critical values of interactions on μ in the absence of Hund's coupling, $J = 0$.

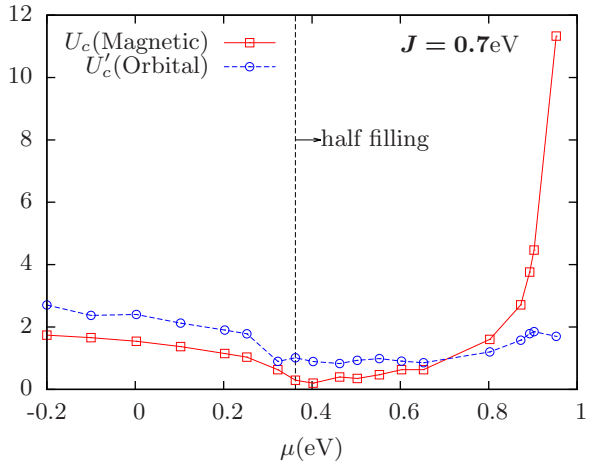

FIG. 6. (Color online) The dependence of critical values of interactions on μ for finite Hund's coupling $J = 0.7$ eV.

At small interaction strength, the spin and orbital susceptibilities are finite. Upon increasing interaction, spin susceptibility at $\mathbf{Q} = (\pi, 0)$ or $(0, \pi)$ and orbital nematic susceptibility at $\mathbf{q} = (0, 0)$ start to diverge in a certain parameter region, implying the tendency towards columnar antiferromagnetic order and ferro orbital nematic order, respectively. The phase boundaries are thus given when the RPA renormalized susceptibilities diverge.

In Fig. 3 and Fig. 4, we set Hund's coupling $J = 0$ and $J = 0.7eV$, respectively. In both phase diagrams, we observe four separate regions: the isotropic paramagnetic phase (PM), the columnar antiferromagnetic phase (CAF), the orbital nematic phase (Orb), and a region where both susceptibilities have diverged (CAF+Orb). In the CAF region, since magnetic order has already developed ($\langle M_1 \rangle \neq \langle M_2 \rangle$), the orbital nematic order should also be nonzero since there is a linear coupling between orbital order and magnetism, see Eq. (2).

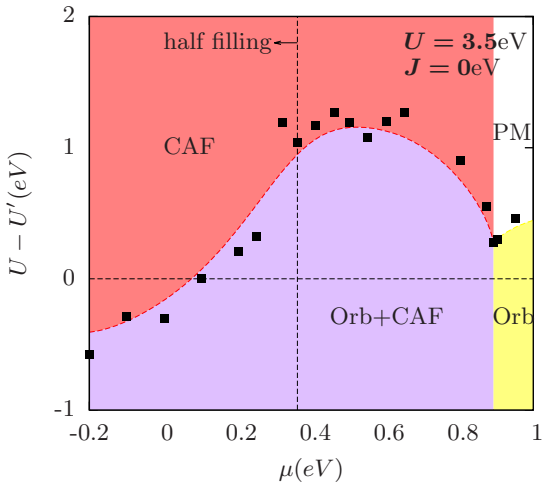

FIG. 7. (Color online) RPA phase diagram when fixing $U = 3.5$eV, $J = 0$. Notice that for sufficiently high electron doping, the orbital nematic phase without magnetic instability (yellow region) appears even when intra-orbital interaction dominates $U > U'$. Dashed vertical line marks the half-filled case (parent compound).

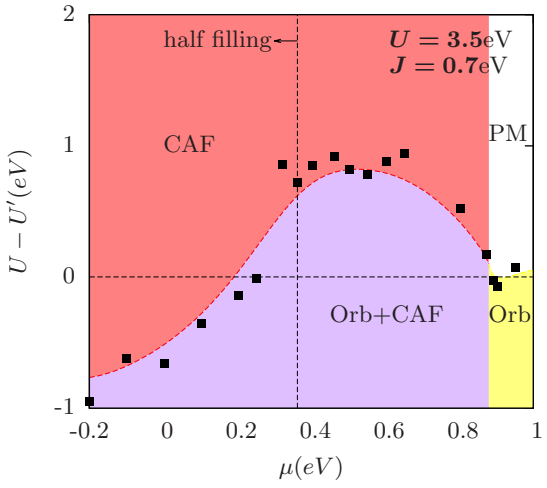

FIG. 8. (Color online) RPA phase diagram when fixing $U = 3.5$eV, $J = 0.7$eV. As in Fig. 7, a non-magnetic orbital nematic phase (yellow region) is stabilized by electron doping. Dashed vertical line marks the half-filled case (parent compound).

We therefore used dashed line in the phase diagrams to indicate that the CAF and CAF+Orb phases are actually not distinguishable. This is not true for the boundary between Orb and CAF+Orb phases however, since finite orbital order ($\langle p \rangle \neq 0$) does not necessarily lead to long-range magnetic order: magnetic fluctuations can break the C_4 symmetry, $\langle \psi \rangle \neq 0$ in Eq. (1), without a true magnetic order[38].

We have also studied the effect of doping on the phase diagram. Let's denote the critical value of U when the system enters the magnetic CAF phase as U_c (while keeping $U' = 0$), and denote the critical value of U' when the system becomes orbitally ordered as U_c' (while keeping $U = 0$).

The dependence of U_c and U_c' on doping is plotted in Fig. 5 for zero Hund's coupling and in Fig. 6 for a realistic value of $J = 0.7$ eV.

From Figs. 5 and 6 we see that both electron and hole doping enhance the critical value of interactions necessary to stabilize antiferromagnetic or orbital order, making it more difficult to enter the ordered phases. However, the doping effect is not particle-hole symmetric: electron doping greatly enlarges U_c, which means that magnetic order is suppressed much faster than orbital nematic order upon electron doping. To make this more transparent, we plotted the phase diagrams describing both the effects of interactions and doping in Fig. 7 and Fig. 8. Besides the effect that larger U' makes the orbital nematic phase more stable, which is consistent with Fig. 3 and Fig. 4, we also notice that the phases are very sensitive to doping. In particular, when the system is sufficiently doped with electrons, we found that the magnetic susceptibility is always finite, so that as a function of increasing $U' - U$, the only phase transition is from paramagnetic phase to the orbital nematic phase, without any magnetism. Interestingly, the orbital ordered phase can be stabilized even when the intra-orbital repulsion U dominates ($U > U'$), see Fig. 7. Normally, the regime $U > U'$ is expected to be dominated by antiferromagnetism (c.f. the half-filled case, marked by a dashed vertical line), however in the case of large electron doping the propensity to magnetic ordering is strongly suppressed, resulting in a non-magnetic orbital nematic phase (yellow region in Figs. 7 and Fig. 8).

IV. VARIATIONAL CLUSTER APPROXIMATION

The RPA is a weak-coupling approach that only detects the tendency to certain orderings based on the divergence of the respective susceptibilities. To study the ordered phases themselves, we use the variational cluster approximation (VCA)[62], which is a non-perturbative quantum cluster method similar in spirit to the cluster dynamical mean-field theory (CDMFT)[63]. Unlike in the CDMFT however, the bath degrees of freedom are not included explicitly in the calculation. Rather, the effect of the bath is captured indirectly by varying the inter-cluster one-body parameters $\{h\}$ in such a way as to minimize the free energy (Potthoff functional) $\Omega[\Sigma_{ij}(\omega)]$ calculated in the conserving approximation[62]. The Potthoff functional depends on the cluster self-energy $\Sigma_{ij}(\omega, \{h\})$, which in turn depends on the variational parameters of the cluster $\{h\}$. These parameters are fixed from the variational principle on the Potthoff functional: $\delta\Omega[\Sigma]/\delta\Sigma = 0$ at the solution. In practical calculations, the variational principle is enforced by requiring that $\partial\Omega[\Sigma(\{h\})]/\partial\{h\} = 0$.

Formulated in this fashion, the VCA is a variational extension of the cluster perturbation theory[64,65] and provides a powerful way of treating the strongly correlated lattice models with local (on-site) interactions. The VCA method has been shown to capture both the weak- and strong-coupling limit of the (one-band) Hubbard model and compares very favourably to the quantum Monter Carlo simulations. It has been used successfully to study the metal-insulator transition[66,67], frustrated magnetism[68,69] and d-wave superconductivity in quasi-2D organic superconductors[70] and in the high-Tc cuprates[68,71,72]. It was shown in particular to capture the d-wave superconductivity of purely electronic origin and to yield the correct doping dependence[72], as well as the pseudogap feature in the quasiparticle spectral weight[71,73]. We use the exact diagonalization (ED) method based on Lanczos method to solve the quantum cluster impurity model, which offers two principal advantages over the Monte-Carlo based solvers routinely used in CDMFT: (i) there is no need for analytical continuation as the self-energy is expressed in real, not imaginary, frequency and (ii) the zero-temperature properties can be readily accessed, avoiding the infamous fermionic sign problem inherent to the quantum Monte Carlo impurity solvers.

The VCA method is particularly well suited to our task because it allows explicit treatment of a spontaneous symmetry-breaking long-range order, and has been successfully used to study magnetism[68,69,74] and unconventional superconductivity[68,71,72] in the Hubbard model. To study the orbital nematic order, we allow the Hamiltonian on a cluster to have a variational degree of freedom associated with a cluster Weiss field, $\Delta\hat{H}_{cl} = p_{\rm cl}\cdot(\hat{n}_{xz} - \hat{n}_{yz})$. Note that the actual lattice Hamiltonian is unaltered, so that the C_4 symmetry is not explicitly broken by construction. Rather, the spontaneously broken symmetry inside the orbital nematic phase is signified by a non-zero value of the cluster Weiss field $p_{\rm cl}$ at the variational solution of the Potthoff functional[62]:

$$\left.\frac{\delta\Omega[\Sigma(p_{\rm cl})]}{\delta p_{\rm cl}}\right|_{\rm sol} = 0. \qquad (18)$$

This is in difference to earlier VCA calculations of nematicity by Daghofer and collaborators[75,76], in which the C_4 tetragonal symmetry was broken by construction at the level of the original lattice Hamiltonian, by introducing anisotropy either in the onsite energy of the xz/yz orbitals, in the hopping amplitudes between the x and y directions, or in the Heisenberg exchange terms in the x and y directions. These studies do not probe the spontaneous symmetry breaking but rather investigate the response of the system to the C_2 distortion, similar in spirit to the experimental studies under uniaxial stress[3] or strain[8]. The present approach, on the other hand, is faithful to the original variational idea by Potthoff[62], allowing the C_4 symmetry to be broken spontaneously, by introducing the in-cluster nematic Weiss field $p_{\rm cl}$.

From the solution of Eq. (18), we then obtain the cluster propagator and self-energy using the ED solver. The full lattice propagator $G(\mathbf{K}, \omega)$ is then calculated from the cluster solution by treating the one-body hopping terms between neighboring clusters as a perturbation. When the Potthoff functional is minimized at a nonzero value of $p_{\rm cl}$, the full lattice Hamiltonian will develop a long range order of the orbital nematicity, ie. a nonzero value of $\langle p\rangle \equiv \langle \hat{n}_{xy} - \hat{n}_{yz}\rangle$.

In Fig. 9, the expectation value of the orbital nematic order parameter is calculated on the lattice, as a function of $U' = U$. After developing a non-zero value of $\langle p\rangle$, upon further increasing $U' = U$, the orbital nematic order parameter attains a peak and then becomes suppressed at higher values of the

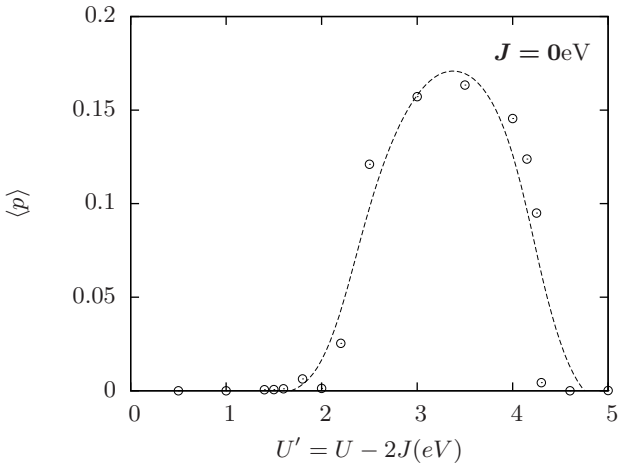

FIG. 9. Orbital nematic order parameter versus interaction strength from VCA calculation at half-filling. The inter-orbital Hubbard repulsion U' is varied at the same time as the intra-orbital U: $U' = U - 2J$, with the Hund's coupling J fixed at zero. The dotted line is a guide to the eye.

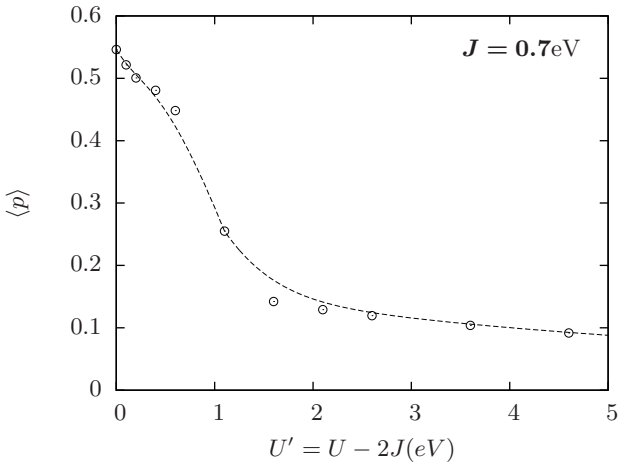

FIG. 10. Orbital nematic order parameter versus the inter-orbital Hubbard coupling $U' = U - 2J$ from VCA calculation at half-filling. Hund's coupling is fixed at $J = 0.7eV$. The dotted line is a guide to the eye.

interaction strength. In the calculation for a realistic value of Hund's coupling $J = 0.7$ eV (Fig. 10), the magnitude of order parameter p starts from a non-zero value when U' is small. This is somewhat unexpected from our RPA results, where Hund's coupling J slightly suppresses orbital nematic order (see Fig. 3, 4, 5 and 6). Upon further increasing U', the same suppression of p is observed as in the case of $J = 0$ above (see Fig. 9).

The above VCA calculations have probed the orbital nematic order in the absence of antiferromagnetism. Of course we know from our RPA calculations that magnetism also arises in the phase diagram of the two-orbital model. The effects of interaction on magnetic order alone (without orbital

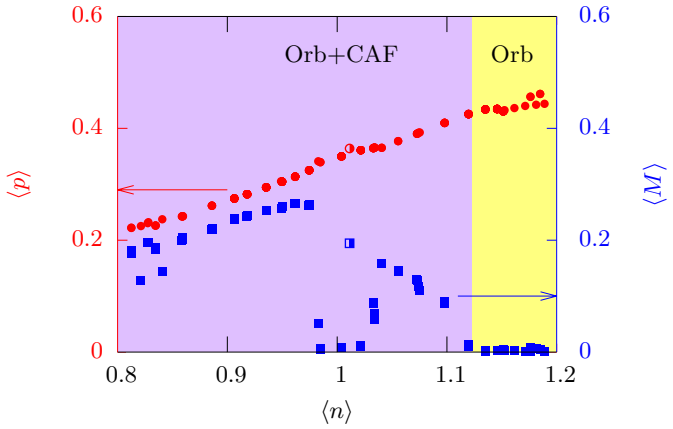

FIG. 11. (Color online) Change of orbital nematic order (circle) and magnetic order(square) with respect to doping from VCA calculation, when $U = 2$ eV, $U' = 0.6$ eV, $J = 0.7$ eV. The half-full symbol corresponds to not a smooth minima but a cusp in the Potthoff functional. Note that near half filling, solutions with zero staggered magnetization appear – these are unphysical and should be disregarded due to the VCA minimization algorithm becoming unstable when the chemical potential falls onto sharp maxima/minima in the density of states.This does not however affect any of our conclusions.

order) have been studied with VCA in Ref. 51. The authors found that the magnetic order starts developing at intermediate interactions U in the parent compounds. (Although it should be noted that in their study, the Hund's coupling J was assumed to scale with U as $J = U/4$, which becomes unphysical for too small or too large values of U).

We will now investigate the phase diagram of the model as a function of electron doping when both the orbital order and columnar antiferromagnetism are present. We set the interaction strengths close to realistic values determined from the *ab initio* constrained-RPA calculations[61]: $U = 2$ eV, $J = 0.7$ eV, $U' = U - 2J = 0.6$ eV. Besides the orbital nematic Weiss field $p_{\rm cl}$ coupled to $n_{xy} - n_{yz}$ on the cluster, we have also introduced the columnar antiferromagnetic Weiss field $M_{\rm cl}$ coupled to $S^z_{\boldsymbol{r}} \cos(\boldsymbol{Q} \cdot \boldsymbol{r})$ on the cluster, with wave vector $\boldsymbol{Q} = (\pi, 0)$ or $(0, \pi)$. A VCA variational search was then performed for both $p_{\rm cl}$ and $M_{\rm cl}$, to study the interplay of the two orders. The resulting doping dependence is plotted in Fig. 11, where the lattice chemical potential was varied to control the electron occupancy. We found coexisting orbital and antiferromagnetic orders in the parent compound at half-filling. While both types of ordering are suppressed by hole doping, the effect of electron doping is to slightly enhance the orbital nematic order while suppressing antiferromagnetism. This effect likely stems from the competition between the two orders, although the enhancement of orbital order with electron doping could be an artifact of the simplified two-orbital model studied here.

Crucially, we find that upon electron doping, antiferromagnetism is suppressed much faster than orbital nematic phase, resulting in a region at sufficiently high electron doping ($x \gtrsim 13\%$) where orbital nematic order exists without any magnetism. This is consistent with our previous RPA finding

(yellow region in Figs. 7 and 8).

V. DISCUSSION

We have studied the emergence of orbital nematic order in the iron pnictide superconductors, within the framework of the two-orbital Hubbard model that captures the physics of Fe d_{xz} and d_{yz} orbitals. In particular, we have analyzed the dependence of the nematic order on doping and interaction strength, as well as its interplay with magnetism.

First, we studied the instabilities towards the orbital nematic order and magnetic order in the weak-coupling approach by calculating the corresponding susceptibilities using the RPA method. We recovered the results of previous studies that the ordering wave-vector is at $\mathbf{Q} = (\pi, 0)$ or $(0, \pi)$ for columnar antiferromagnetism[50] and $(0, 0)$ for ferro-orbital nematic order[28], respectively. We found that orbital nematic order strongly depends on inter-orbital Hubbard repulsion U', while magnetic order depends on the intra-orbital Hubbard repulsion U. Both the magnetic and orbital nematic order parameters are affected by Hund's coupling J: larger J values tend to suppress the propensity to orbital nematic ordering and, on the other hand, enhance the magnetic susceptibility.

It has been long believed that the nematicity and antiferromagnetism coexist at low temperatures, with a wealth of experimental data supporting this in the 1111 and 122 families of iron pnictides. Within the RPA, we indeed find regions in the phase space where both the magnetic and nematic susceptibilities diverge, implying coexistence of the two order parameters. It is true that the long-range CAF phase with $M_1 \neq M_2$ (the notation introduced in Sec. I) necessarily breaks the C_4 symmetry and will generically induce a non-zero value of orbital polarization p because of the linear coupling in the Landau free energy. The converse is however not true: the ferro-orbital phase with non-vanishing p, while nematic in nature, need not have long-range magnetic order. Indeed, our RPA calculations show that upon electron doping, magnetic susceptibility is suppressed much faster than orbital ordering, until for sufficiently large electron doping, only orbital order survives (See Fig. 5 and Fig. 6). Hole doping, on the other hand, does not reveal this tendency.

We note that our results do not eliminate the possibility of spin fluctuations taking part in the nematicity even if the static magnetic order is absent. Indeed, as remarked in the Introduction, ferro-orbital nematic order parameter will couple linearly to the spin-fluctuation Ising parameter, see Eq. (2). However, when the system is sufficiently far from the antiferromagnetic phase, as is arguably the case in FeSe[45,46], spin fluctuations are expected to be weak, whereas a non-zero static ferro-orbital order will be the main driver of the nematicity.

Since RPA is a weak coupling approach which works only when the long-range order is approached from the disordered phase, we have used the non-perturbative variational cluster approximation (VCA) which allowed us to study the ordered phases in the variational approach. We studied the orbital nematic and magnetic order parameters, as well as their interplay as a function of electron density (doping) and interaction strength. Our VCA calculation showed that orbital nematic order strongly depends on inter-orbital Hubbard interaction U' and Hund's coupling J, similar to the RPA results. However, while Hund's coupling suppresses orbital order within the RPA approach, this is not the case in the non-perturbative VCA calculation. In Fig. 10, we find a non-vanishing orbital nematic order even in the absence of inter-orbital interaction $U' = 0$ and finite Hund's coupling $J = 0.7$ eV, implying that the effect of interactions and Hund's term is not always captured properly by the RPA method.

The doping dependence study from VCA shows that electron and hole doping are not symmetric. Crucially, we find that upon moderate electron doping ($\gtrsim$ 13%, see Fig. 11), long-range magnetic order is completely suppressed, while the orbital nematic order persists, similar to our RPA results.

It is instructive to compare our VCA results with previous attempts to address nematicity with the cluster dynamical mean-field theory (CDMFT)[63] and similar cluster approaches. One possible way to detect tendency to nematicity is to explicitly introduce orthorhombic distortion into the hopping terms in Eqs. (4, 5), and then study the electronic response. For the one-band Hubbard model, this has been done using CDMFT[77] and dynamical cluster approximation[78]. Both groups found that for a sufficiently large interaction U, a small orthorhombic distortion can lead to a large nematic response in the low-energy electron scattering rate. Another way to study the spontaneous development of nematicity in the one-band Hubbard model is by introducing an anisotropic hopping inside the cluster alone $\Delta\hat{H}_{cl} = \delta t \sum_{\boldsymbol{r}} (\hat{c}^{\dagger}_{\boldsymbol{r}} \hat{c}_{\boldsymbol{r}+x} - \hat{c}^{\dagger}_{\boldsymbol{r}} \hat{c}_{\boldsymbol{r}+y}) + h.c.$, and then optimize the strength of δt variationally in VCA[79]. Using this approach, the authors found that anisotropy can develop in the overdoped region.[79] However, the multi-orbital nature of the iron pnictides was not taken into account in these studies.

The nematicity in multi-band Hubbard model has been studied with VCA in Refs. 75 and 76, however these authors have also explicitly broken the C_4 tetragonal symmetry at the level of the original lattice Hamiltonian, by introducing anisotropy either in the onsite energy of the xz/yz orbitals, in the hopping amplitudes between the x and y directions, or in the Heisenberg exchange terms in the x and y directions. Because the C_4 symmetry is broken by construction, these studies do not probe the spontaneous symmetry breaking but rather investigate the response of the system to the C_2 distortion, similar in spirit to the experimental studies under uniaxial stress[3] or strain[8]. Not surprisingly, the magnitude of the induced orbital order is then proportional to the imposed strain and does not have an intrinsic value. In the present work, by contrast, the lattice expectation value of orbital order $p = \langle \hat{n}_{xz} - \hat{n}_{yz} \rangle$ is finite even at zero induced strain and is consistent with the value found by ARPES in $BaFe_2As_2$ [23].

We note that in a different context, nematicity in a two-orbital Hubbard model has also been studied in application to $Sr_3Ru_2O_7$ in Refs. 80 and 81. In these works, the authors studied the nematic instability using RPA and renormalization group methods. It was found that Aslamazov–Larkin-type vertex corrections result in the strong coupling between spin and orbital fluctuations, leading the authors to conclude

that the spin fluctuations lie at the origin of the nematic instability. In the present work, on the other hand, we find a regime of parameters where the ferro-orbital RPA susceptibility diverges even without the vertex corrections, while the spin susceptibility remains finite (see section III). This implies that the spin fluctuations are not the primary origin of ferro-orbital nematicity in our model. Furthermore, from our VCA calculations we find that the orbital nematic order persists even when magnetic ordering is fully suppressed in the electron doped region (see Fig. 11), which again suggests that magnetic fluctuations are not the origin of orbital nematicity in our case. It should be noted that the Fermi surface topology and nesting properties in $Sr_3Ru_2O_7$ are different from the iron pnictices, so the conclusions drawn in Refs. 80, 81 do not trivially generalize to our case.

Finally, we note that other types of orbital ordering, involving d_{xy} orbitals, have been proposed in the literature,[7,35,82] however those are beyond the scope of the two-orbital model used in this study. While it would be desirable to extend this study to include all five iron orbitals, unfortunately the VCA calculations become computationally prohibitive because of the limitations of the exact diagonalization solver when dealing with multiple orbitals. Nevertheless, as remarked earlier in Sec. II, we hope that the present two-orbital model captures the salient features of nematicity in the iron pnictides, based on the dominant contribution of d_{xz} and d_{yz} orbitals to the Fermi surfaces of these materials.[53]

VI. CONCLUSIONS

To summarize, we have studied the doping dependence of both the orbital nematic and antiferromagnetic orders using the RPA and non-perturbative variational cluster approximation, and found a region at moderately large electron doping where the orbital nematic order survives without long-range magnetism. While these results are limited to the two-orbital model, which is not sufficient to describe the realistic band structure of the iron-based superconductors, our findings are suggestive of the connection to the experimental observations of an orbital nematic phase in FeSe[47–49] without any sign of antiferromagnetism.[45,46] This raises the question whether two-fold symmetric antiferromagnetic fluctuations are essential for stabilizing the nematic phase, as has been argued previously within the spin-nematic scenario.[27,39–41,57] It would appear from the present study that this may not always be the case, and while the importance of spin fluctuations is undeniable in the vicinity of the magnetic order in the 122 and 1111 families of iron pnictides, it is the orbital fluctuations that appear to be critical for the onset of nematicity in FeSe. This situation may be more common than previously appreciated: recent ARPES measurements[52] detect d_{xz}/d_{yz} orbital splitting inside the superconducting phase in the parent LiFeAs as well as electron-doped $LiFe_{1-x}Co_xAs$, with no magnetic phase nearby. Very recently, orbital ordering has also been observed[83] inside the superconducting phase of the optimally doped and overdoped $BaFe_2(As_{1-x}P_x)_2$, far away from the magnetically ordered phase and in the same regime where the torque magnetometry detected C_2-symmetric spin response[21]. These observations also raise the question of the interplay between orbital nematicity and superconductivity in the iron pnictides, which will be the subject of future study.

ACKNOWLEDGMENTS

We are grateful to David Sénéchal for his help with the VCA method, and we are indebted to Andrei Chubukov for many fruitful discussions. We acknowledge discussions with Steve Kivelson, Yuji Matsuda, Abhay Pasupathy, Ian Fisher, Rafael Fernandes and Matthew Foster. This work was performed with partial support from the Welch foundation grant, C-1818. A.H.N. acknowledges the hospitality of the Aspen Center for Physics (NSF grant #1066293) where part of this work has been performed.

[1] Y. Kamihara, T. Watanabe, M. Hirano, and H. Hosono, Journal of the American Chemical Society **130**, 3296 (2008)
[2] Z.-A. Ren, W. Lu, J. Yang, W. Yi, X.-L. Shen, Z.-C. Li, G.-C. Che, X.-L. Dong, L.-L. Sun, F. Zhou, and Z.-X. Zhao, Chin. Phys. Lett **25**, 2215 (2008)
[3] J.-H. Chu, J. G. Analytis, K. De Greve, P. L. McMahon, Z. Islam, Y. Yamamoto, and I. R. Fisher, Science **329**, 824 (2010)
[4] M. A. Tanatar, E. C. Blomberg, A. Kreyssig, M. G. Kim, N. Ni, A. Thaler, S. L. Bud'ko, P. C. Canfield, A. I. Goldman, I. I. Mazin, and R. Prozorov, Phys. Rev. B **81**, 184508 (May 2010)
[5] E. C. Blomberg, M. A. Tanatar, A. Kreyssig, N. Ni, A. Thaler, R. Hu, S. L. Bud'ko, P. C. Canfield, A. I. Goldman, and R. Prozorov, Phys. Rev. B **83**, 134505 (Apr 2011)
[6] H.-H. Kuo, J.-H. Chu, S. C. Riggs, L. Yu, P. L. McMahon, K. De Greve, Y. Yamamoto, J. G. Analytis, and I. R. Fisher, Phys. Rev. B **84**, 054540 (Aug 2011)
[7] J. J. Ying, X. F. Wang, T. Wu, Z. J. Xiang, R. H. Liu, Y. J. Yan, A. F. Wang, M. Zhang, G. J. Ye, P. Cheng, J. P. Hu, and X. H. Chen, Phys. Rev. Lett. **107**, 067001 (Aug 2011)
[8] J.-H. Chu, H.-H. Kuo, J. G. Analytis, and I. R. Fisher, Science **337**, 710 (2012)
[9] S. Jiang, H. S. Jeevan, J. Dong, and P. Gegenwart, Phys. Rev. Lett. **110**, 067001 (Feb 2013)
[10] S. Ishida, M. Nakajima, T. Liang, K. Kihou, C. H. Lee, A. Iyo, H. Eisaki, T. Kakeshita, Y. Tomioka, T. Ito, and S. Uchida, Phys. Rev. Lett. **110**, 207001 (May 2013)
[11] M. Nakajima, T. Liang, S. Ishida, Y. Tomioka, K. Kihou, C. H. Lee, A. Iyo, H. Eisaki, T. Kakeshita, T. Ito, and S. Uchida, Proceedings of the National Academy of Sciences **108**, 12238 (2011)
[12] A. Dusza, A. Lucarelli, A. Sanna, S. Massidda, J.-H. Chu, I. R. Fisher, and L. Degiorgi, New Journal of Physics **14**, 023020 (2012)
[13] M. Nakajima, S. Ishida, Y. Tomioka, K. Kihou, C. H. Lee, A. Iyo, T. Ito, T. Kakeshita, H. Eisaki, and S. Uchida, Phys. Rev. Lett. **109**, 217003 (Nov 2012)

[14] T.-M. Chuang, M. P. Allan, J. Lee, Y. Xie, N. Ni, S. L. Budko, G. S. Boebinger, P. C. Canfield, and J. C. Davis, Science **327**, 181 (2010)

[15] X. Zhou, C. Ye, P. Cai, X. Wang, X. Chen, and Y. Wang, Phys. Rev. Lett. **106**, 087001 (Feb 2011)

[16] M. P. Allan, T.-M. Chuang, F. Massee, Y. Xie, N. Ni, S. L. Bud'ko, G. S. Boebinger, Q. Wang, D. S. Dessau, P. C. Canfield, M. S. Golden, and J. C. Davis, Nat Phys **9**, 220 (2013)

[17] L. W. Harriger, H. Q. Luo, M. S. Liu, C. Frost, J. P. Hu, M. R. Norman, and P. Dai, Phys. Rev. B **84**, 054544 (Aug 2011)

[18] H. Luo, M. Wang, C. Zhang, X. Lu, L.-P. Regnault, R. Zhang, S. Li, J. Hu, and P. Dai, Phys. Rev. Lett. **111**, 107006 (Sep 2013)

[19] X. Lu, J. T. Park, R. Zhang, H. Luo, A. H. Nevidomskyy, Q. Si, and P. Dai, Science(2014), in print

[20] T. Terashima, N. Kurita, M. Tomita, K. Kihou, C.-H. Lee, Y. Tomioka, T. Ito, A. Iyo, H. Eisaki, T. Liang, M. Nakajima, S. Ishida, S.-i. Uchida, H. Harima, and S. Uji, Phys. Rev. Lett. **107**, 176402 (Oct 2011)

[21] S. Kasahara, H. J. Shi, K. Hashimoto, S. Tonegawa, Y. Mizukami, T. Shibauchi, K. Sugimoto, T. Fukuda, T. Terashima, A. H. Nevidomskyy, and Y. Matsuda, Nature **486**, 382 (2012)

[22] T. Shimojima, K. Ishizaka, Y. Ishida, N. Katayama, K. Ohgushi, T. Kiss, M. Okawa, T. Togashi, X.-Y. Wang, C.-T. Chen, S. Watanabe, R. Kadota, T. Oguchi, A. Chainani, and S. Shin, Phys. Rev. Lett. **104**, 057002 (Feb 2010)

[23] M. Yi, D. Lu, J.-H. Chu, J. G. Analytis, A. P. Sorini, A. F. Kemper, B. Moritz, S.-K. Mo, R. G. Moore, M. Hashimoto, W.-S. Lee, Z. Hussain, T. P. Devereaux, I. R. Fisher, and Z.-X. Shen, Proceedings of the National Academy of Sciences **108**, 6878 (2011)

[24] T. Shimojima, T. Sonobe, W. Malaeb, K. Shinada, A. Chainani, S. Shin, T. Yoshida, S. Ideta, A. Fujimori, H. Kumigashira, K. Ono, Y. Nakashima, H. Anzai, M. Arita, A. Ino, H. Namatame, M. Taniguchi, M. Nakajima, S. Uchida, Y. Tomioka, T. Ito, K. Kihou, C. H. Lee, A. Iyo, H. Eisaki, K. Ohgushi, S. Kasahara, T. Terashima, H. Ikeda, T. Shibauchi, Y. Matsuda, and K. Ishizaka, Phys. Rev. B **89**, 045101 (Jan 2014)

[25] C. Fang, H. Yao, W.-F. Tsai, J.-P. Hu, and S. A. Kivelson, Phys. Rev. B **77**, 224509 (Jun 2008)

[26] C. Xu, M. Müller, and S. Sachdev, Phys. Rev. B **78**, 020501 (Jul 2008)

[27] J. Dai, Q. Si, J.-X. Zhu, and E. Abrahams, Proceedings of the National Academy of Sciences **106**, 4118 (2009)

[28] C.-C. Lee, W.-G. Yin, and W. Ku, Phys. Rev. Lett. **103**, 267001 (Dec 2009)

[29] W. Lv, J. Wu, and P. Phillips, Phys. Rev. B **80**, 224506 (Dec 2009)

[30] C.-C. Chen, B. Moritz, J. van den Brink, T. P. Devereaux, and R. R. P. Singh, Phys. Rev. B **80**, 180418 (Nov 2009)

[31] F. Krüger, S. Kumar, J. Zaanen, and J. van den Brink, Phys. Rev. B **79**, 054504 (Feb 2009)

[32] C.-C. Chen, J. Maciejko, A. P. Sorini, B. Moritz, R. R. P. Singh, and T. P. Devereaux, Phys. Rev. B **82**, 100504 (Sep 2010)

[33] W. Lv, F. Krüger, and P. Phillips, Phys. Rev. B **82**, 045125 (Jul 2010)

[34] B. Valenzuela, E. Bascones, and M. J. Calderón, Phys. Rev. Lett. **105**, 207202 (Nov 2010)

[35] H. Kontani, T. Saito, and S. Onari, Phys. Rev. B **84**, 024528 (Jul 2011)

[36] H.-H. Kuo and I. R. Fisher(2013), arXiv:1311.0933

[37] C. de la Cruz, Q. Huang, J. W. Lynn, J. Li, W. R. II, J. L. Zarestky, H. A. Mook, G. F. Chen, J. L. Luo, N. L. Wang, and P. Dai, Nature **453**, 899 (2008)

[38] P. Chandra, P. Coleman, and A. I. Larkin, Phys. Rev. Lett. **64**, 88 (1990)

[39] R. M. Fernandes, E. Abrahams, and J. Schmalian, Phys. Rev. Lett. **107**, 217002 (Nov 2011)

[40] R. M. Fernandes and J. Schmalian, Superconductor Science and Technology **25**, 084005

[41] R. M. Fernandes, A. V. Chubukov, and J. Schmalian, Nature Phys. **10**, 97 (2014)

[42] M. Yi, D. H. Lu, R. G. Moore, K. Kihou, C.-H. Lee, A. Iyo, H. Eisaki, T. Yoshida, A. Fujimori, and Z.-X. Shen, New Journal of Physics **14**, 073019 (2012)

[43] Y. Zhang, C. He, Z. R. Ye, J. Jiang, F. Chen, M. Xu, Q. Q. Ge, B. P. Xie, J. Wei, M. Aeschlimann, X. Y. Cui, M. Shi, J. P. Hu, and D. L. Feng, Phys. Rev. B **85**, 085121 (Feb 2012)

[44] E. P. Rosenthal, E. F. Andrade, C. J. Arguello, R. M. Fernandes, L. Y. Xing, X. C. Wang, C. Q. Jin, A. J. Millis, and A. N. Pasupathy, Nat Phys **10**, 225 (2014)

[45] T. M. McQueen, A. J. Williams, P. W. Stephens, J. Tao, Y. Zhu, V. Ksenofontov, F. Casper, C. Felser, and R. J. Cava, Phys. Rev. Lett. **103**, 057002 (Jul 2009)

[46] M. Bendele, A. Amato, K. Conder, M. Elender, H. Keller, H.-H. Klauss, H. Luetkens, E. Pomjakushina, A. Raselli, and R. Khasanov, Phys. Rev. Lett. **104**, 087003 (Feb 2010)

[47] T. Shimojima, Y. Suzuki, T. Sonobe, A. Nakamura, M. Sakano, J. Omachi, K. Yoshioka, M. Kuwata-Gonokami, K. Ono, H. Kumigashira, A. E. Böhmer, F. Hardy, T. Wolf, C. Meingast, H. von Löhneysen, H. Ikeda, and K. Ishizaka, (unpublished) arXiv:1407.1418(2014)

[48] S. H. Baek, D. V. Efermov, J. M. Ok, J. S. Kim, J. van den Brink, and B. Büchner, (unpublished) arXiv:1408.1875(2014)

[49] A. E. Böhmer, T. Arai, F. Hardy, T. Hattori, T. Iye, T. Wolf, H. von Löhneysen, K. Ishida, and C. Meingast, (unpublished) arXiv:1407.5497(2014)

[50] S. Raghu, X.-L. Qi, C.-X. Liu, D. J. Scalapino, and S.-C. Zhang, Phys. Rev. B **77**, 220503 (Jun 2008)

[51] M. Daghofer, A. Moreo, J. A. Riera, E. Arrigoni, D. J. Scalapino, and E. Dagotto, Phys. Rev. Lett. **101**, 237004 (Dec 2008)

[52] H. Miao, L.-M. Wang, P. Richard, S.-F. Wu, J. Ma, T. Qian, L.-Y. Xing, X.-C. Wang, C.-Q. Jin, C.-P. Chou, Z. Wang, W. Ku, and H. Ding, Phys. Rev. B **89**, 220503 (Jun 2014)

[53] S. Graser, T. A. Maier, and P. J. Hirschfeld, New J. Phys. **11**, 025016 (2009)

[54] M. Daghofer, A. Nicholson, A. Moreo, and E. Dagotto, Phys. Rev. B **81**, 014511 (2010)

[55] K. Kuroki, S. Onari, R. Arita, H. Usui, Y. Tanaka, H. Kontani, and H. Aoki, Phys. Rev. Lett. **101**, 087004 (Aug 2008)

[56] R. M. Fernandes, L. H. VanBebber, S. Bhattacharya, P. Chandra, V. Keppens, D. Mandrus, M. A. McGuire, B. C. Sales, A. S. Sefat, and J. Schmalian, Phys. Rev. Lett. **105**, 157003 (Oct 2010)

[57] R. M. Fernandes, A. V. Chubukov, J. Knolle, I. Eremin, and J. Schmalian, Phys. Rev. B **85**, 024534 (Jan 2012)

[58] A. V. Chubukov, Ann. Rev. Cond. Matter Phys. **3**, 57 (2012)

[59] E. Gull, A. J. Millis, A. I. Lichtensitein, A. N. Rubtsov, T. M., and P. Werner, Rev. Mod. Phys. **83**, 349 (2011)

[60] E. Dagotto, T. Hotta, and A. Moreo, Physics Reports **344**, 1 (2001)

[61] M. Aichhorn, L. Pourovskii, V. Vildosola, M. Ferrero, O. Parcollet, T. Miyake, A. Georges, and S. Biermann, Phys. Rev. B **80**, 085101 (Aug 2009)

[62] M. Potthoff, M. Aichhorn, and C. Dahnken, Phys. Rev. Lett. **91**, 206402 (Nov 2003)

[63] G. Kotliar, S. Y. Savrasov, G. Pálsson, and G. Biroli, Phys. Rev. Lett. **87**, 186401 (Oct 2001)

[64] C. Gros and R. Valentí, Phys. Rev. B **48**, 418 (Jul 1993)

[65] D. Sénéchal, D. Perez, and M. Pioro-Ladrière, Phys. Rev. Lett. **84**, 522 (Jan 2000)
[66] M. Balzer, W. Hanke, and M. Potthoff, Phys. Rev. B **77**, 045133 (Jan 2008)
[67] M. Balzer, B. Kyung, D. Snchal, A.-M. S. Tremblay, and M. Potthoff, EPL (Europhysics Letters) **85**, 17002
[68] A. H. Nevidomskyy, C. Scheiber, D. Sénéchal, and A.-M. S. Tremblay, Phys. Rev. B **77**, 064427 (Feb 2008)
[69] P. Sahebsara and D. Sénéchal, Phys. Rev. Lett. **100**, 136402 (Mar 2008)
[70] P. Sahebsara and D. Sénéchal, Phys. Rev. Lett. **97**, 257004 (Dec 2006)
[71] D. Sénéchal and A.-M. S. Tremblay, Phys. Rev. Lett. **92**, 126401 (Mar 2004)
[72] D. Sénéchal, P.-L. Lavertu, M.-A. Marois, and A.-M. S. Tremblay, Phys. Rev. Lett. **94**, 156404 (Apr 2005)
[73] A.-M. S. Tremblay, B. Kyung, and D. Snchal, Low Temperature Physics **32** (2006)
[74] C. Dahnken, M. Aichhorn, W. Hanke, E. Arrigoni, and M. Potthoff, Phys. Rev. B **70**, 245110 (Dec 2004)
[75] M. Daghofer, A. Nicholson, and A. Moreo, Phys. Rev. B **85**, 184515 (May 2012)
[76] M. Daghofer and A. Fischer, Supercond. Sci. Technol. **25**, 084003 (2012)
[77] S. Okamoto, D. Sénéchal, M. Civelli, and A.-M. S. Tremblay, Phys. Rev. B **82**, 180511(R) (Nov 2010)
[78] S.-Q. Su and T. A. Maier, Phys. Rev. B **84**, 220506 (Dec 2011)
[79] K. Fang, G. W. Fernando, and A. N. Kocharian, Journal of Physics: Condensed Matter **25**, 205601 (2013)
[80] M. Tsuchiizu, Y. Ohno, S. Onari, and H. Kontani, Phys. Rev. Lett. **111**, 057003 (Jul 2013)
[81] Y. Ohno, M. Tsuchiizu, S. Onari, and H. Kontani, Journal of the Physical Society of Japan **82**, 013707 (2013)
[82] S. Onari and H. Kontani, Phys. Rev. Lett. **109**, 137001 (Sep 2012)
[83] T. Sonobe *et al.*, unpublished (private communication)